Tectonophysics xxx (2010) xxx–xxx

Contents lists available at ScienceDirect

Tectonophysics

journal homepage: www.elsevier.com/locate/tecto

The 2004–2005 Les Saintes (French West Indies) seismic aftershock sequence observed with ocean bottom seismometers

S. Bazin [a,b,c,*], N. Feuillet [c,d], C. Duclos [b,c], W. Crawford [b,1], A. Nercessian [e], M. Bengoubou-Valérius [a,f], F. Beauducel [a,e], S.C. Singh [b]

[a] Observatoire Volcanologique et Sismologique de Guadeloupe, IPGP, 97113 Gourbeyre, Guadeloupe, French West Indies
[b] Géosciences Marines, IPGP, CNRS-INSU, 4 place Jussieu, 75005 Paris, France
[c] Observatoire Volcanologique et Sismologique de Martinique, IPGP, 97250, Fonds Saint-Denis, Martinique, French West Indies
[d] Tectonique et Mécanique de la Lithosphère, IPGP, CNRS-INSU, 4 place Jussieu, 75005 Paris, France
[e] Sismologie, IPGP, CNRS-INSU, 4 place Jussieu, 75005 Paris, France
[f] BRGM Guadeloupe, 97113 Gourbeyre, Guadeloupe, French West Indies

ARTICLE INFO

Article history:
Received 18 December 2009
Received in revised form 12 March 2010
Accepted 9 April 2010
Available online xxxx

Keywords:
Ocean bottom seismometer
Local earthquake tomography
Normal-fault earthquake
Aftershock sequence
Fault–fluid interactions
Les Saintes
Lesser Antilles

ABSTRACT

On November 21, 2004 an M_w6.3 intraplate earthquake occurred at sea in the French Caribbean. The aftershock sequence continues to this day and is the most extensive sequence in a French territory in more than a century. We recorded aftershocks from day 25 to day 66 of this sequence, using a rapidly-deployed temporary array of ocean bottom seismometers (OBS). We invert P- and S-wave arrivals for a tomographic velocity model and improve aftershock locations. The velocity model shows anomalies related to tectonic and geologic structures beneath the Les Saintes graben. 3D relocated aftershocks outline faults whose scarps were identified as active in recent high-resolution marine data. The aftershocks distribution suggests that both the main November 21 event and its principal aftershock, on February 14, 2005, ruptured Roseau fault, which is the largest of the graben, extending from Dominica Island to the Les Saintes archipelago. Aftershocks cluster in the lower part of the Roseau fault plane (between 8 and 12.6 km depth) that did not rupture during the main event. Shallower aftershocks occur in the Roseau fault footwall, probably along smaller antithetic faults. We calculate a strong negative Vp anomaly, between 4 and 8 km depth, within the graben, along the Roseau fault plane. This low Vp anomaly is associated with a high Vp/Vs ratio and may reflect a strongly fracturated body filled with fluids. We infer from several types of observation that fault lubrication is the driving mechanism for this long-lasting aftershock sequence.

1. Introduction

On November 21, 2004, an M_w6.3 earthquake struck the Les Saintes archipelago (Guadeloupe, French West Indies). The earthquake epicenter was located 15 km south-east of the Les Saintes (Guadeloupe, French West Indies). This is the largest earthquake recorded in the Lesser Antilles arc since the 1985 M_w6.2 Redonda earthquake, offshore Montserrat Island (Girardin et al., 1991). It killed one child and was felt with a maximum intensity of VIII in the Les Saintes archipelago (Cara et al., 2005). It is the most damaging earthquake in a French territory since the 1967 M_w 5.1 Arette event (intensity VIII, (Cara et al., 2008)). A strong M_w5.8 aftershock occurred on February 14, 2005 and the aftershock sequence continues to this day. There is still debate about which fault or faults ruptured during this on-going sequence. In order to better study the aftershocks, six ocean bottom seismometers (OBS) were deployed around the active zone 25 days after the main event. The OBS array was deployed for 41 days, recording up to 250 events per day. In this paper, we present the results of a simultaneous inversion of the aftershock arrivals for event hypocenters and 3D subsurface velocities.

2. Seismotectonic setting

Along the Lesser Antilles arc, the North American and South American plates dip beneath the Caribbean plate at a rate of 2 cm/yr in a WSW direction (DeMets et al., 2000). As a consequence, the Eastern Caribbean is prone to a moderate to large seismic hazard (Bernard and Lambert, 1988). Three types of damaging seismicity can be distinguished in the arc (Stein et al., 1982). The first type is directly related to the subduction at the plate interface. The second type is within the subducting slab at greater depth. The third type of seismicity, which we study here, occurs within the Caribbean plate. Deformation within the Caribbean plate is accommodated by normal and oblique faults (Feuillet et al., 2001, 2004). A large en echelon fault system running

* Corresponding author. Temporarily at: International Centre for Geohazards/ Norwegian Geotechnical Institute, P.O. Box. 3930 Ullevål Stadion, Oslo N-0806, Norway.
E-mail address: bazin@ipgp.fr (S. Bazin).
[1] Temporarily at: Institut de Recherche pour le Développement, c/o Dept Geology and Mines, Private Mail Bag 9001, Port Vila, Vanuatu

0040-1951/$ – see front matter © 2010 Elsevier B.V. All rights reserved.
doi:10.1016/j.tecto.2010.04.005

from north of Montserrat Island to Dominica Island cuts active subaerial volcanoes (Soufrière Hills on Montserrat and Soufrière volcano on Guadeloupe) as well as submarine volcanoes (Fig. 1, (Feuillet, 2000; Feuillet et al., 2001)). These arc parallel normal faults have steep scarps that can reach up to several tens of meters high. The main fault segments dip toward the NE.

Between Guadeloupe and Dominica islands, a 15 km wide, N135°E striking graben belonging to the en echelon fault system was mapped during the AGUADOMAR marine survey (Feuillet, 2000; Feuillet et al., in revision). The graben is bounded by Roseau fault to the SW and the smaller Rodrigues fault to the NE (Fig. 2). The Les Saintes graben crosscuts several underwater volcanic edifices (Roseau and Colibri) which are probably no longer active. The 21 November earthquake occurred along the Les Saintes fault system. Field observations, the aftershock distribution, Coulomb stresses and tsunami modelling present Roseau fault as the best candidate for the mainshock rupture (Beauducel et al., 2005; Le Friant et al., 2008; Feuillet et al., in revision). It is the largest fault of the graben running 18 km in length with a cumulative scarp of up to 120 m (Feuillet, 2000). The centroid moment tensors (CMT) computed by the Harvard and Geoscope groups show a dominant normal-faulting mechanism with a slight strike–slip component. The two focal mechanisms do not differ by much (Table 1 and Fig. 2) and are compatible with the Roseau fault azimuth.

More than 30000 events were recorded by the Earthquake and Volcano Observatory of Guadeloupe (OVSG-IPGP) during the 5 years following the main event (Beauducel et al., 2005; IPGP, 2009). At the time of the main shock and the first days of aftershocks, the precision

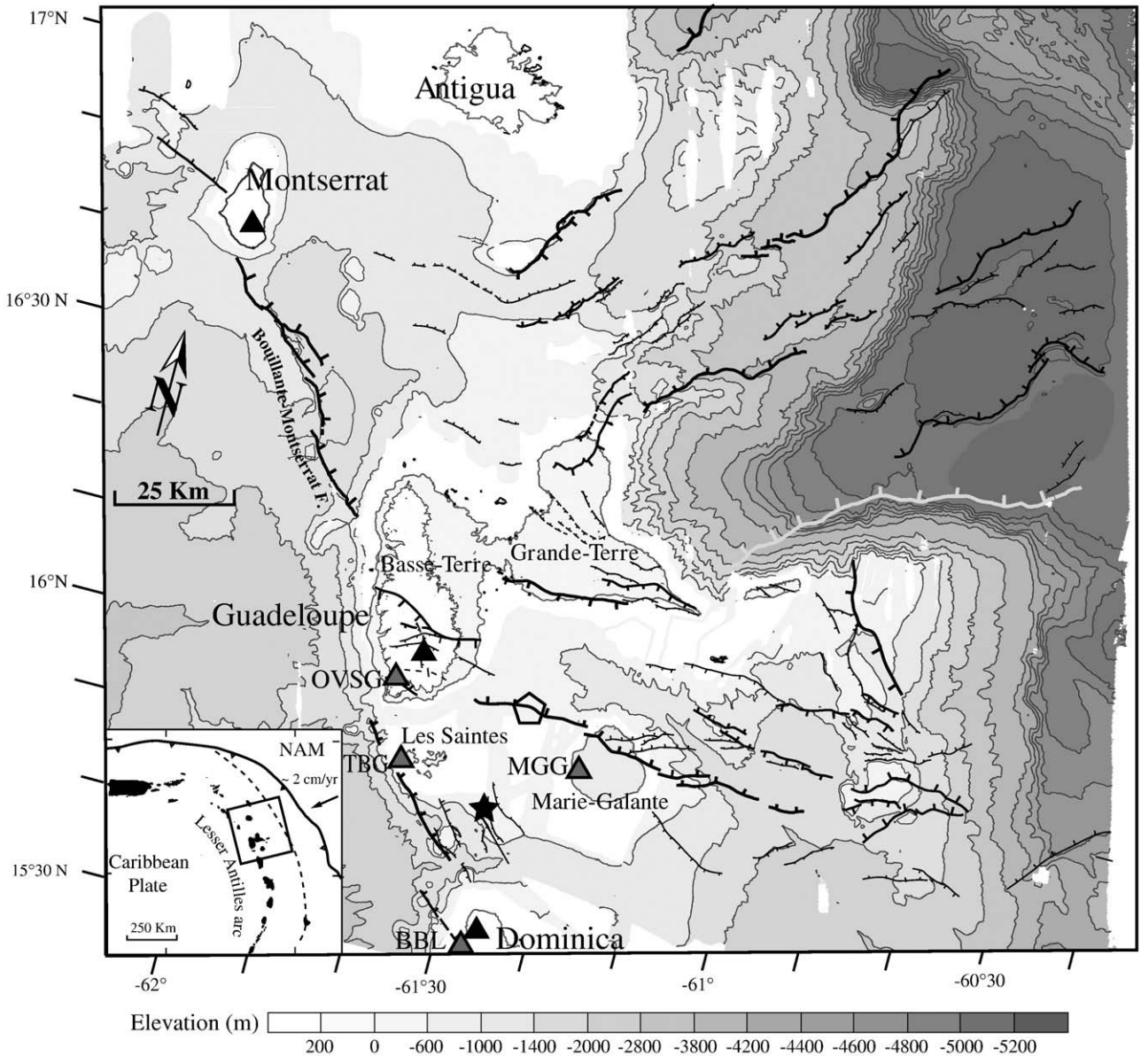

Fig. 1. Map of Guadeloupe Island along the East Caribbean volcanic arc (modified from Feuillet et al., 2004). The M_w6.3 earthquake discussed here occurred at sea between Guadeloupe and Dominica Islands, 15 km south-east of the Les Saintes archipelago (epicenter displayed as star). Black triangles indicate active volcanoes. The main seismic stations of the regional network are BBL in northern Dominica, MGG on Marie-Galante Island, and the Soufrière volcano seismic network south of Basse-Terre (regrouped under OVSG on this map). MGG was the closest station to the mainshock, 27 km away. A permanent vertical seismometer TBG was installed on Terre de Bas Island in the Les Saintes archipelago a few days after the mainshock, which improved the network's local detection threshold and location accuracy. The pentagone indicates the region where a geyser was observed by Blainville in 1843 (Bouysse, 1980) on Morne–Piton fault (cf Appendix A). The inset displays the Lesser Antilles arc at the eastern boundary of the Caribbean plate. The vector indicates the convergence rate between North American and Caribbean plates (DeMets et al., 2000).

Please cite this article as: Bazin, S., et al., The 2004–2005 Les Saintes (French West Indies) seismic aftershock sequence observed with ocean bottom seismometers, Tectonophysics (2010), doi:10.1016/j.tecto.2010.04.005

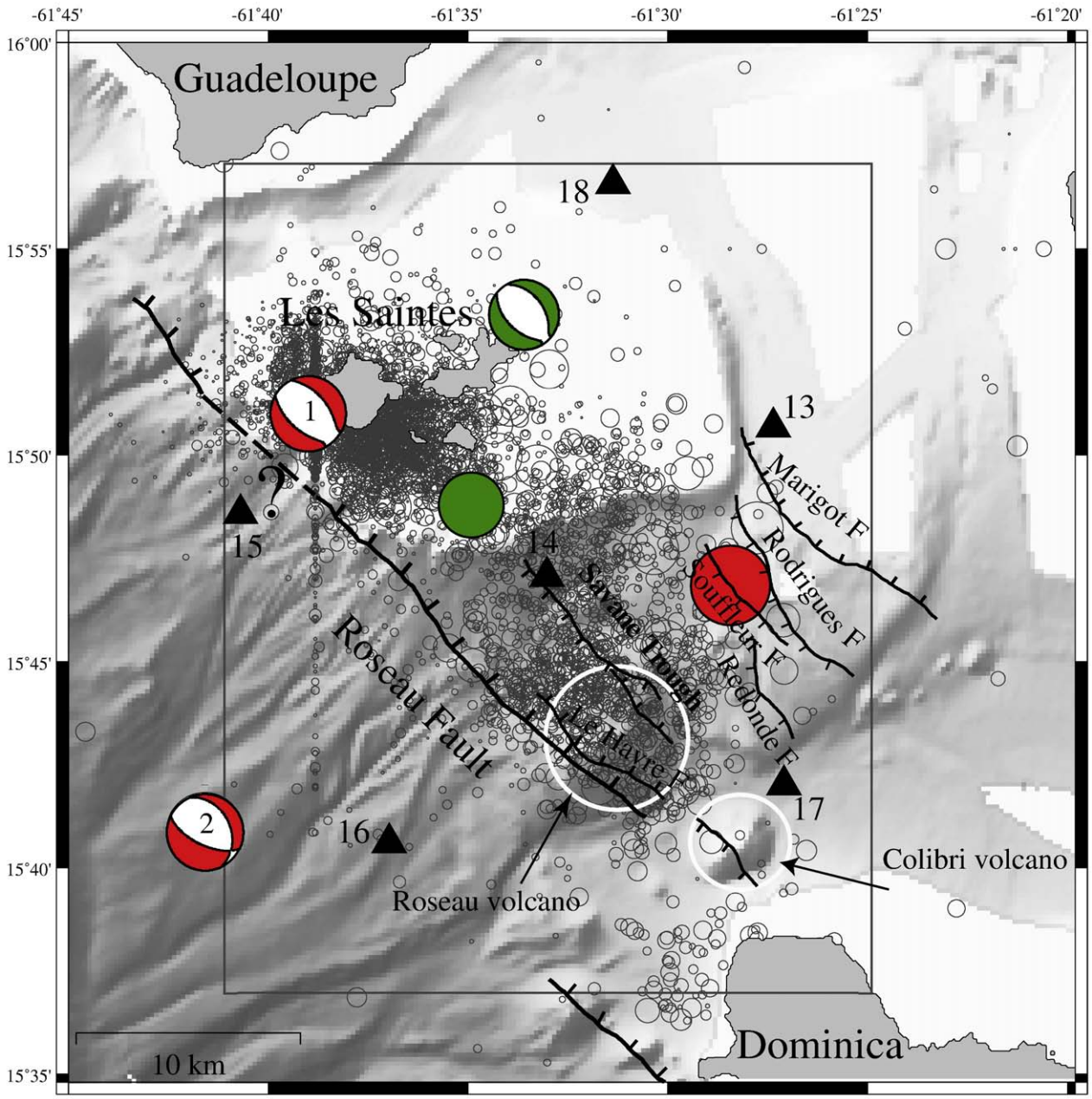

Fig. 2. Locations of the 5547 aftershocks manually picked by OVSG seismologists between 21 November 2004 and 17 September 2009 (IPGP, 2009). The data collected during this swarm is so voluminous, especially during the first year, that the whole period has not been processed. These preliminary locations present artefacts due to the limited monitoring array. The aftershocks distribution is cloudy but reveals a seismic gap near 15°47′N, which we will discuss below. Magnitudes detected are between 1 and 5.8, hypocentral depths range from the surface to 34 km with an average depth of 8.6 km. Position errors are 2.9 km horizontally. The filled red circle marks the mainshock as initially located by the OVSG network (15.77°N, 61.48°W, 14.5 km depth). Red beach balls show CMT and epicenters for the mainshock (1 is Harvard and 2 is Geoscope solution). The filled green circle marks the main aftershock as located by the OVSG network (15.81°N, 61.58°W, 11.7 km). The Harvard CMT solution for the main aftershock is displayed in green beach ball symbol. Underwater volcanoes are marked and the simplified fault scarps from Feuillet (2000) show the geometry of a graben in the channel between Guadeloupe and Dominica Islands. Les Saintes Islands are plotted above the seismicity symbols for clarification. Bathymetry relief in grey shading is from AGUADOMAR cruise (Deplus et al., 2001). Regions above 200 m below sea level, were not mapped, not permitting fault mapping on the Les Saintes insular shelf. Hence, the northern end of Roseau fault was not mapped, it may continue and connect to a branch mapped NW of the plateau. The triangles show the positions of the six OBS deployed after the mainshock for this study. The grey box delineates the area of map views of the velocity model shown in Fig. 8.

and detection threshold of the permanent network was limited by its geometry. In general, the alignment of monitoring stations along the island arc makes it difficult to accurately locate earthquakes in the EW direction. Several seismological networks located the November 21, 2004 event but positions differ by more than 15 km (Fig. 2 and Bertil et al. (2004)). More than 2000 events were detected during the first day. Seismic activity decreased very rapidly during the first week and more progressively after the first two months. The aftershocks form an elongated pattern, 22 km long and 10 km wide, following the graben azimuth and covering the whole fault system (Fig. 2). The aftershocks located by the permanent network do not indicate a clear fault plane and they cluster in two regions: one located beneath the Les Saintes islands and the other beneath the submarine Roseau volcano. The activity of this southern cluster faded through time and, 5 years later, only the cluster underneath Les Saintes remains active (IPGP, 2009; Feuillet et al., in revision).

Please cite this article as: Bazin, S., et al., The 2004–2005 Les Saintes (French West Indies) seismic aftershock sequence observed with ocean bottom seismometers, Tectonophysics (2010), doi:10.1016/j.tecto.2010.04.005

Table 1
CMT solutions.

Event	Solution	Moment (N m)	NP1 Strike	NP1 Dip	NP1 Rake	NP2 Strike	NP2 Dip	NP2 Rake
21 Nov 2004	Harvard[a]	$3.44\ 10^{18}$	325°	44°	−77°	127°	48°	102°
	Geoscope[b]	$4.63\ 10^{18}$	334°	34°	−54°	115°	63°	−112°
14 Feb 2005	Harvard[a]	$0.698\ 10^{18}$	326°	41°	−79°	132°	50°	−99°

[a] Global Centroid Moment Tensor database, formerly known as the Harvard CMT catalog: http://www.globalcmt.org/CMTsearch.html.
[b] Computed by E. Clévédé and G. Patau with IPGP-INSU data from http://www.geosp6.ipgp.jussieu.fr/CMT/Default_cmt_previous.htm.

3. Data and technique

To better locate aftershocks and determine the fault responsible for the main event, we deployed an array of six OBSs around the Les Saintes graben from 16 December 2004 to 25 January 2005, using the Ports and Lighthouses vessel *Kahouanne*. The OBSs are from an instrument pool owned by the Institut National des Sciences de l'Univers (INSU) and operated by the Institut de Physique du Globe de Paris (IPGP, http://www.ipgp.fr/pages/02120601.php). Each OBS is composed of a Hitech HYI-90-U hydrophone and a Mark Products L-22 vertical geophone mounted in a separate pressure case. The OBSs are designed by the Scripps Institution of Oceanography: detailed descriptions of the L-Cheapo package are given by Constable et al. (1998) and are available at http://www.obsip.org. The OBSs recorded at 125 samples per second per channel. Five OBSs encircled the active zone and one was placed in the center of the network to better constrain aftershock depths. The analysis of OBS data requires more pre-processing than for land stations because the instruments can neither be positioned or time synchronized by GPS while they are at the seafloor. A GPS time synchronization is made just before and just after deployment, and a linear drift correction applied. The OBS clock drift rates ranged from 11 to 37 ms during the 41 days of deployment (0.3–0.9 ms/day before correction). The drifts of the OBS Seascan clocks are typically rated to <0.5 ms/day. We estimate the OBS coordinates and depths by inverting travel times of direct water wave arrivals. The initial coordinates are taken from GPS coordinates of the instrument drop locations and the initial instrument depths are taken from sonar soundings or derived by interpolating the bathymetry grid at the drop locations. We sent acoustic pings from the vessel within a radius of 2.5 km around each instrument in order to triangulate for their position and depth. New instrument coordinates and depths as well as the average velocity in the water column are estimated using least-squares fit of travel times through the water column. The instruments experienced lateral drifts from 16 to 77 m during descent, the drift distance being proportional to the water depth at the drop site. Estimated water column velocities range from 1520 m/s to 1582 m/s. These velocities are inversely proportional to the water depth at the drop site and are compatible with regional conductivity-temperature–depth (CTD) profiles. The data recovery is 100% for the six OBS and the data quality is generally good, but we observe a puzzling monochromatic noise centered at 6.35 Hz on all geophones (Fig. 3). This noise is not recorded by any of the six hydrophones, nor by the land seismometers. It is almost continuous on OBS 15 and less intensive on OBS 13 and 18. It occurs only twice a day in average for OBS 14, 16 and 17. These monochromatic infrasound waves are not correlated in time with seismicity and do not occur simultaneously on all geophones. We believe that the noise source was localized at the seafloor. A similar 6–7 Hz noise was recorded offshore of Equator by geophones with a different design than our sensors. Pontoise and Hello (2002) interpreted them as methane seepage from underwater canyons due to erosion processes. They suggested a model for pressure waves resulting from oscillating clouds of bubbles.

The OBS recorded continuous data during 41 days of active seismicity. More than 4000 events are detected using an automated software running on the Earthworm platform (open source developed by USGS, see http://www.isti2.com/ew for details) based on an STA^3/LTA^4 algorithm originally developed by Allen (1978). A visual selection removes interfering signals and seismic events from other regions. Events are then manually picked using the Seisan software package (see Havskov and Ottemöller, 2005). P- and associated S-time arrivals are carefully checked using the Wadati (1933) method. Generally, S-wave arrivals are difficult to read because their onset lies in the P-wave coda and their amplitude is usually not much greater than that of the P-wave arrival. Having the two channels with the vertical geophone and the hydrophone helps the picking. A total of 3905 earthquakes are manually picked, of which 3767 had enough arrival time picks to be located. The picking accuracy is on the order of 0.024 s for the P coda and 0.048 s for the S coda.

During the same period, the OVSG permanent monitoring network recorded 392 events. OVSG seismologists routinely calculate earthquake magnitude using the duration form of Lee and Lahr (1975): $M_d = 2\log T + 0.0035D - 0.87$, where T (s) is the time lag between the P-wave arrival time and the end of the S coda, log is logarithm to the base 10, and D (km) is the epicentral distance. This local scale has been in use since the first seismological bulletins in this network. According to Bengoubou-Valérius et al. (2008) the M_d scale is shifted by 0.1 to 0.2 below the m_b computed by the USGS for magnitude above 4. Five significant events occurred during the OBS experiment: on 19 December (M_d4.0), 21 December (M_d4.2), 26 December (M_d4.5), 27 December (M_d4.8) and 10 January (M_d4.3). M_d estimation is impossible on the OBS dataset so we used the maximum amplitude of the S coda, following a method developed by the Japan Meteorological Agency (JMA) for shallow earthquake monitoring. JMA has been publishing local magnitudes using the empirical form: $M_l = a\ \log A + b\ \log D + c$ where a, b, and c are constants, log is logarithm to the base 10, A is the maximum velocity amplitude, and D (km) is the epicentral distance (JMA, 2004). We use a minimum least-squares search algorithm to determine the values of a, b and c best fitting the M_d values of the OVSG database. The coefficients obtained for the JMA empirical formula are $a = 1.15$, $b = 1.42$ and $c = -6.12$ and the magnitude distribution for the 3542 events is shown on Fig. 4a. The M_l values range from −0.7 to 4. For $M_d \geq 3.5$, the OBS geophones generally saturate and no M_l value is assigned to the event. The local magnitude of completeness is on the order of 1 for the OBS array, while the regional value is 2.7 (Bengoubou-Valérius et al., 2008). A Gutenberg-Richter cumulative curve reveals a b-value of 0.94 during this period (Fig. 4b).

4. 1D velocity model

The velocity model used for the OVSG permanent network was derived from a seismic refraction survey (Dorel et al., 1974; Dorel, 1978). The land station network was not dense at the time and the shot interval was only 15 km, limiting the resolution of the refraction method. This velocity model was the only one available before our study. It was averaged for land and oceanic regions of the Lesser Antilles (Table 2). Although Dorel (1978) computed a regional Vp/Vs value of 1.85, the OVSG routinely uses 1.76 after a recent analysis of

Fig. 3. Monochromatic noise recorded on the OBS geophones. a) Raw signal recorded on the vertical geophone of OBS 15. Left: a representative 2 min time window without earthquake; Right: a representative 34 min time window with many aftershocks. The noise needs to be filtered out to allow accurate picking. b) Spectral analysis of the two time-windows. The fundamental peak, at 6.35 Hz, is visible for both time periods. c) Sonograms of the two time-windows. Two overtones are visible, at 12.7 and 19 Hz. The amplitude of the principal peak and overtones does not correlate with the occurrence of aftershocks. d) Occurrence of the monochromatic noise on each OBS over 1 week. The noise was almost continuous on OBS 15 and less intensive on OBS 13 and 18. It only occurred about twice a day for OBS 14, 16 and 17. e) Corrosion on the OBS metallic parts after recovery from the seafloor.

Please cite this article as: Bazin, S., et al., The 2004–2005 Les Saintes (French West Indies) seismic aftershock sequence observed with ocean bottom seismometers, Tectonophysics (2010), doi:10.1016/j.tecto.2010.04.005

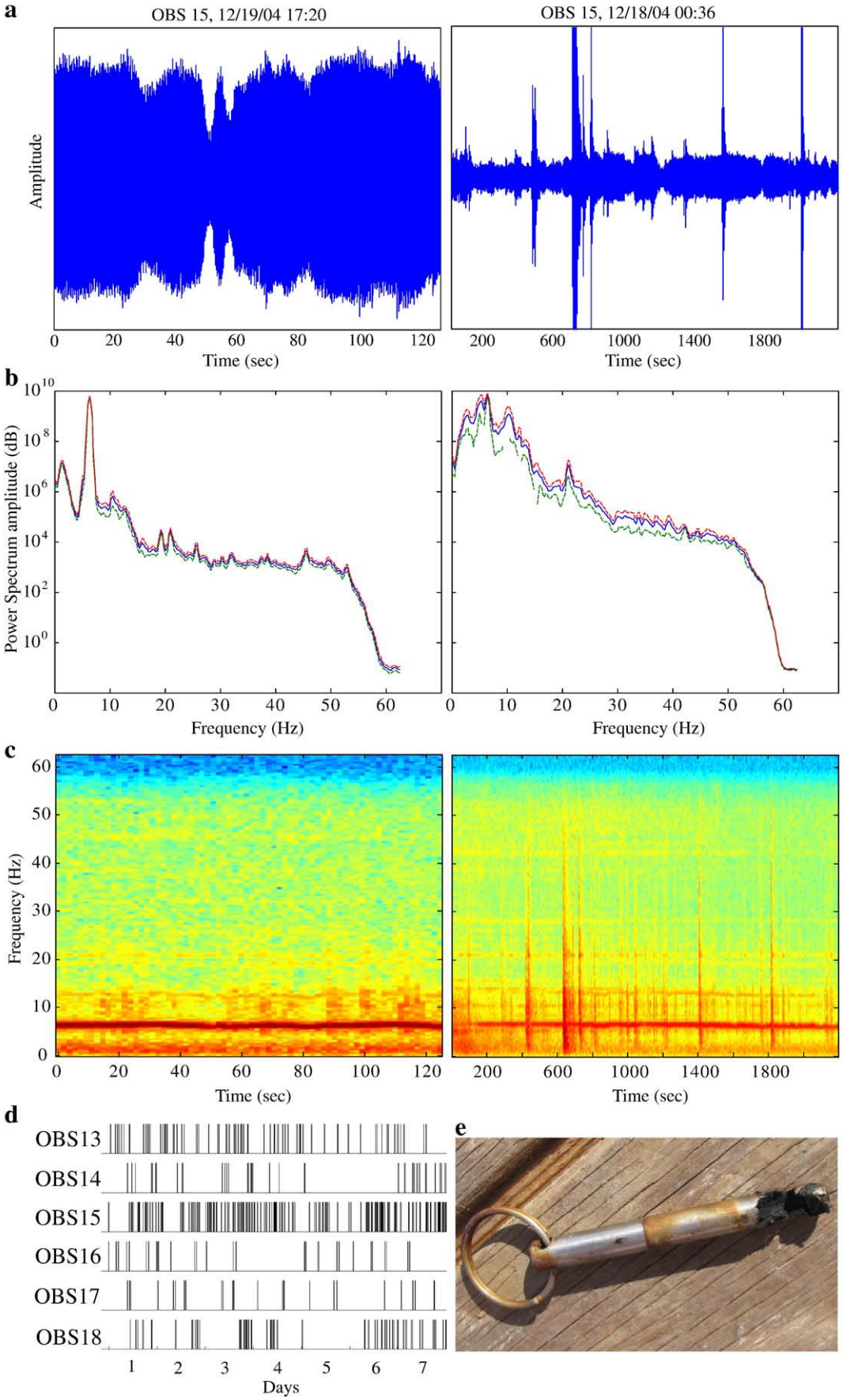

Please cite this article as: Bazin, S., et al., The 2004–2005 Les Saintes (French West Indies) seismic aftershock sequence observed with ocean bottom seismometers, Tectonophysics (2010), doi:10.1016/j.tecto.2010.04.005

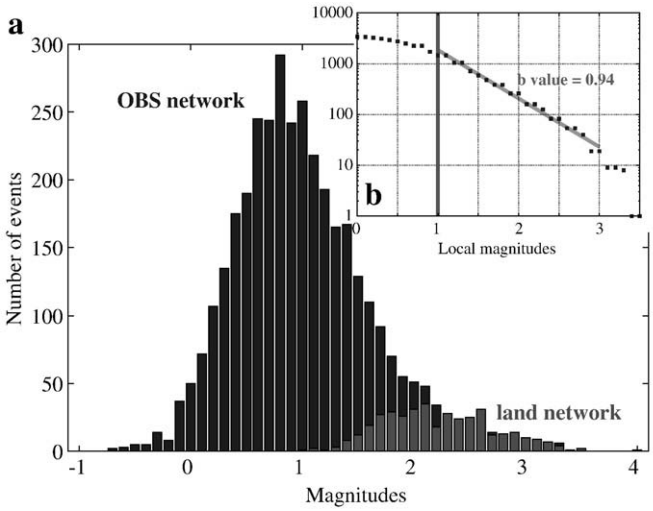

Fig. 4. a) Magnitude distribution of earthquakes recorded by the OBS and the permanent land network over the same 41-day period. The OBS array is sensitive to 9 times more events than the land network. b) Frequency-magnitude distribution for earthquakes recorded by the temporary OBS array. The *b*-value is calculated for events with $M_l \geq 1$, which is the magnitude of completeness of the OBS dataset. The *b*-value was 0.94 during this very active period.

the historical database (Clément et al., 2001). Preliminary earthquake locations using the same velocity model and Vp/Vs as the OVSG are computed for the 3767 OBS events that have sufficient P- and S-arrival times. Localized events are spread over the entire graben (Fig. 5a) and it is difficult to distinguish any clear feature from vertical profiles (therefore sections are not included here). In order to better constrain earthquake locations and to improve the layered velocity model, the data are inverted for a 1D model of velocity versus depth. Events with more than 3 P-S time lags, azimuth coverage ≥ 180° are initially selected. An additional data selection is achieved by slightly varying the velocity model and computing hypocentral shift (a proxy for real hypocentral error, (Lienert, 1994)). Only a subset of data with real epicentral error <2 km and real depth error <3 km are used for the 1D inversion. Travel times from these 1288 events (6225 rays) are inverted using the Velest code (see Kissling et al., 1995) and Dorel (1978) velocity profile as the starting model. The inversion simultaneously computes hypocenters and seismic velocities. The selected events are split into two subsets and each subset was run through the inversion (Kissling et al., 1994). The velocity models and RMS (root mean square) residuals obtained using the two subsets are quite similar which verifies the uniqueness of the solution: the two velocity models differ by 9% at the most and the starting travel-time RMS was reduced from 0.152 s to 0.101 s for the first selection and from 0.158 s to 0.108 s for the second selection. In Fig. 6, we show the two computed 1D velocity models compared to the a-priori one. The so-called minimum 1D model (Table 2) is chosen as that with the lowest RMS travel-time residual of the two subsets. We then test the dependence of the inverted model on the starting model, using high-velocity (+1 km/s) and low-velocity (−1 km/s) starting models (Fig. 6).

We compute hypocenters for the whole dataset using our minimum 1D model. A comparison of hypocenters obtained with the Dorel (1978) model and our inverted velocities (Fig. 5a, b) show a marked improvement in the clustering of events with the new 1D model. Using the Wadati (1933) method, the mean Vp/Vs value is 1.81 with a standard variation of ±0.1.

5. 3D modelling

To compute Vp and Vp/Vs anomalies and further improve earthquake locations, we calculate a 3D velocity model using the local earthquake tomography (LET) algorithm Simul2000 (Thurber, 1983; Eberhart-Phillips, 1990; Eberhart-Phillips and Reyners, 1997). Simul2000 iteratively solves for Vp, Vp/Vs, and updated earthquake locations and origin times. We space velocity nodes 5 km apart in the horizontal and 1 to 3 km apart in the vertical. The damping parameter has an important effect on tomography results: we select the optimum value by following the method described by Evans et al. (1994). We run one inversion iteration for 20 damping values from 1 to 1000. For each damping value, we compute the model complexity and data variance. The damping value of 12 gives the best trade-off between both properties (Fig. 7). Weaker damping would give a more complex velocity model without significantly better fitting the travel-time data. We begin by selecting a subset of 1183 earthquakes of the 1288 already selected for the 1D inversion (the original selection is S phases ≥3, epicentral error <2 km and depth error <3 km), by adding a threshold of 0.25 s for the localization RMS and 180° for the minimum azimuth coverage. As a starting model, we use the minimum 1D model, including its started Vp/Vs ratio of 1.81. The number of observations is 11063 (6630 P- and 4433 S-wave first arrival times) and we inverted for 255 velocity nodes.

Table 2
Compressional velocity depth models used in this study.

Dorel (1978)		Minimum 1D	
Depth (km)	Vp (km/s)	Depth (km)	Vp (km/s)
0–3	3.5	0–1	2.7
		1–2	3.6
		2–3	3.9
3–15	6.0	3–5	5.1
		5–9	5.5
		9–11	5.8
		11–13	5.9
15–30	7.0	13–30	7.0
30+	8.0	30+	8.0

The inversion reduces the RMS travel-time residual from 0.095 s to 0.053 s and the data variance from 0.009 s^2 to 0.003 s^2 after six iterations. Horizontal slices of the 3D velocity model solutions at upper and mid-crustal depths show the internal structure of the Les Saintes graben (Fig. 8). Vertical sections perpendicular to the faults direction reveal anomalies in the vicinity of the faults (Fig. 9). The final Vp velocity model (Figs. 8a, 9a) is highly variable (anomaly ranging between −19 and +13%), whereas Vp/Vs (Figs. 8b, 9b) is less variable (from −6 to +7 %). The Vp/Vs heterogeneity observed in the 3D model (−6 to +7% of 1.81) is on the same order of magnitude as the standard deviation of the minimum 1D model (±0.1). Moreover, the minimum and maximum values for the Vp anomaly (i.e. −19% and +13%) match the discrepancies between the 1D minimum model and the two end-members using high initial velocities and low initial velocities, which do not exceed 1 km/s in the middle crust (Fig. 6). The most striking features are the positive Vp/Vs anomaly in most of the graben region and the negative Vp/Vs anomaly SE of the Les Saintes Islands. A wide negative Vp anomaly of −19% lies between 4 and 8 km depth at the graben center, which at depth tracks the Roseau fault plane. At 6 km depth the Vp anomaly inversely mirrors the Vp/Vs anomaly and we will analyse this observation in the discussion about faulting processes. A very shallow positive Vp anomaly lies SE of the Les Saintes islands, which we interpret as an effect of the reef platform (Fig. 8a, plate $z = 2$ km). A positive Vp anomaly lies 10 km deep near the SE end of the aftershock swarm, *N* of Roseau volcano (Fig. 8a, plate $z = 10$ km). This +10 to +15% anomaly could be related to a frozen magmatic intrusive body.

Different tools exist to verify the LET solution quality and estimate the resolving power of the data set (Kissling et al., 2001). A simple evaluation of the resolution of the 3D seismic model can be obtained from the distribution of ray paths. The hit count distribution sums up the number of rays that contribute to the solution at each node. It

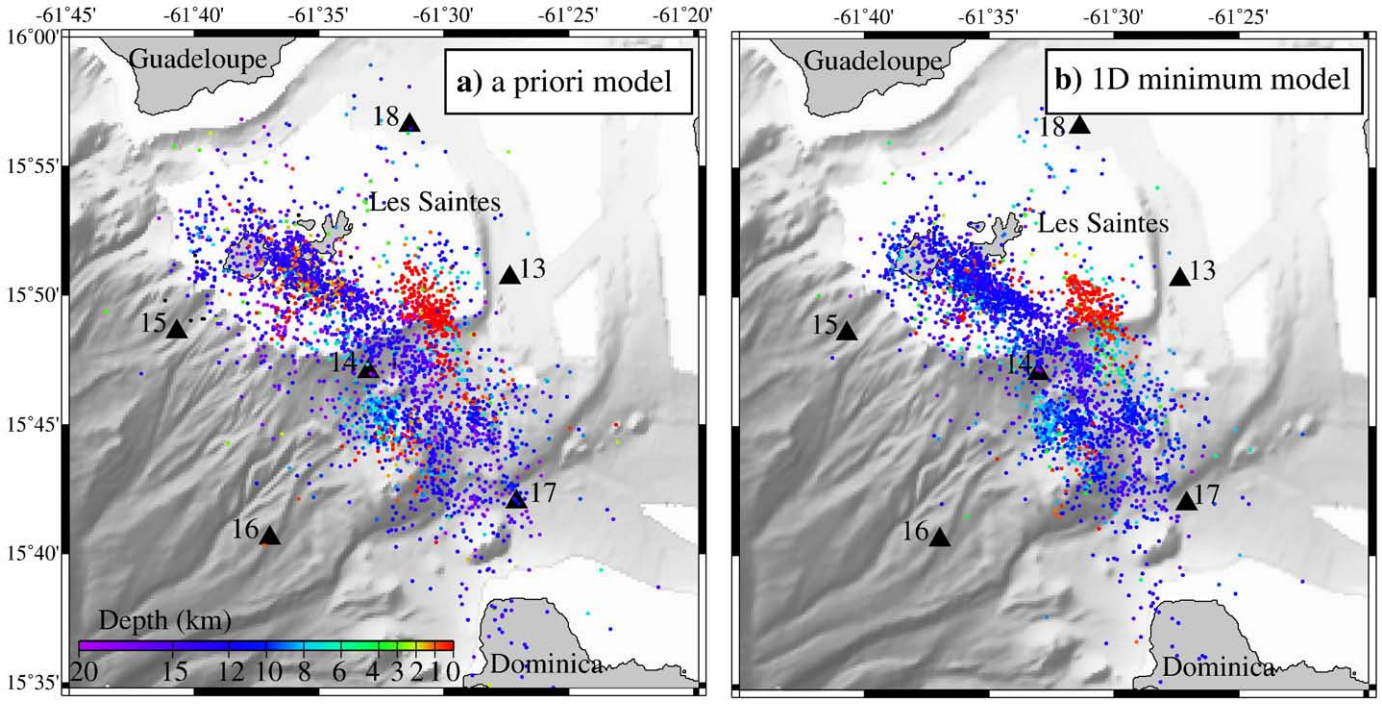

Fig. 5. Map of the seismicity recorded by the temporary OBS array preliminary located using 1D velocity models. The triangles show the positions of the six OBS. Les Saintes and Dominica coastlines are plotted, a) using the 1D velocity model of Dorel (1978). This regional model is the one routinely used for OVSG hypocenter localisations, b) using the minimum 1D model.

outlines the ray coverage but cannot assess the validity of the inversion parameterization. Hit count varies from 2000 to 8000 in most of our model volume. The derivative weight sum (DWS, see Toomey et al.(1994)) are interpreted as a measure of the density of seismic rays influencing each model parameter and therefore outlines the model resolving power. DWS distributions are shown in map views at six depths including those of our velocity model solutions (Fig. 10). The diagonal elements of the resolution matrix (RDE) can also be used as they describe how independent the solution is for one model parameter. It is common to define well-resolved models when RDE >0.2 (e.g. Haslinger et al., 1999). After analyzing the resolution matrix, we define the solution as reliable for areas with a DWS over 5000. This is a conservative choice as areas with DWS >5000 always verify RDE >0.2 in our model. The resolving power is adequate within the OBS array, and is best between 4 and 8 km depth.

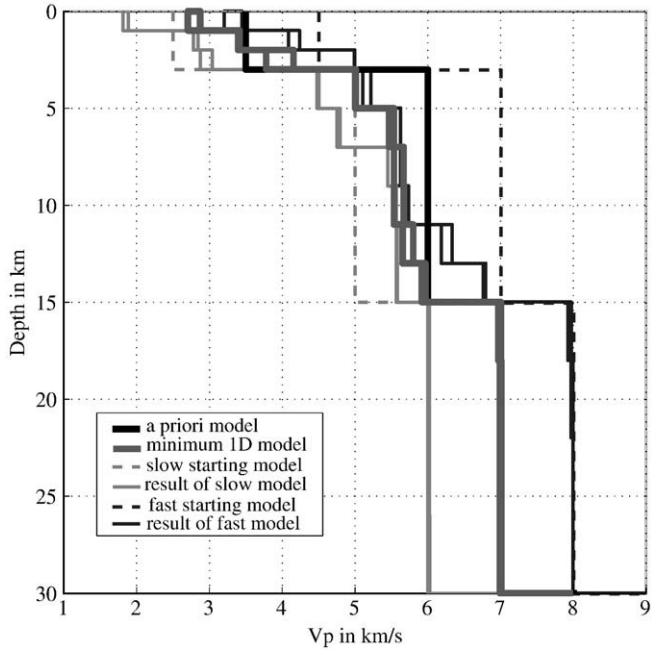

Fig. 6. Comparison of compressional velocity versus depth models from a regional study (thick black line from Dorel (1978)) and the models obtained using the Velest inversion. The solutions for the two subsets of data (two thick dark grey lines) are very similar; this verifies the uniqueness of the solution. The dependence on the starting model is tested using high-velocity and low-velocity starting models. Both solutions (thin black and thin pale grey lines) converge towards the minimum 1D model.

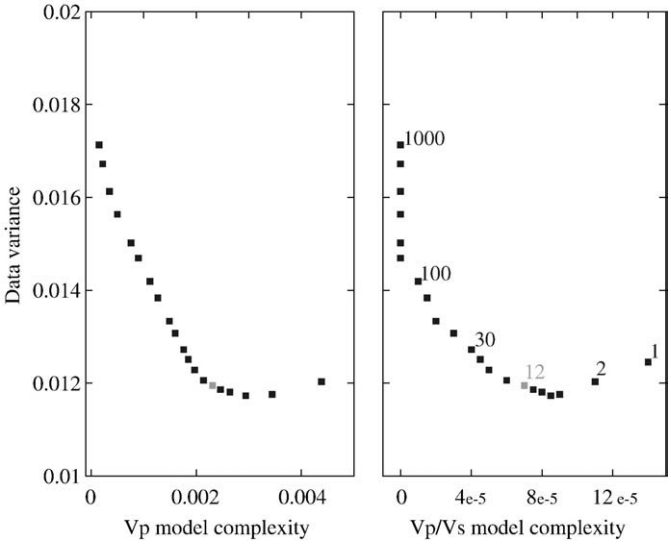

Fig. 7. The effect of damping on the relationship between data variance and model complexity. 20 damping values from 1 to 1000 are tested, the best trade-off between variance and complexity is obtained for a damping parameter value of 12.

Please cite this article as: Bazin, S., et al., The 2004–2005 Les Saintes (French West Indies) seismic aftershock sequence observed with ocean bottom seismometers, Tectonophysics (2010), doi:10.1016/j.tecto.2010.04.005

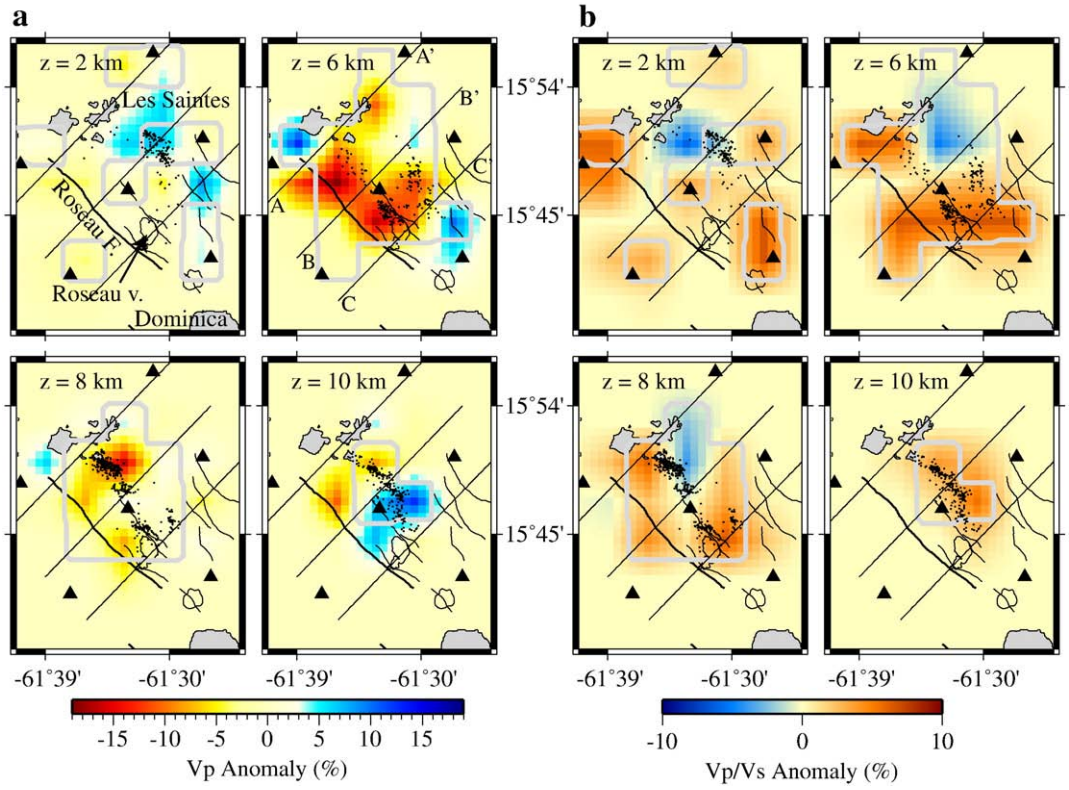

Fig. 8. Map views of the velocity anomalies on four constant-depth planes in the upper crust, mid crust and lower crust. Blue colors represent fast P-wave velocities or low Vp/Vs ratios, while red colors represent slow velocities or high Vp/Vs ratios. The grey lines are the isolines of the well-resolved regions (DWS > 000, see Fig. 10). LET hypocenters located near to each plane are plotted in black (in order, from 0–4, 4–7, 7–9 and 9+ km depth). Black lines mark the positions of the three vertical profiles presented in Fig. 9. Triangles show the OBS positions. The coastlines of the Les Saintes group and Dominica Island, and, the faults and the contour of the underwater volcanoes are plotted. a) Vp anomaly, b) Vp/Vs anomaly.

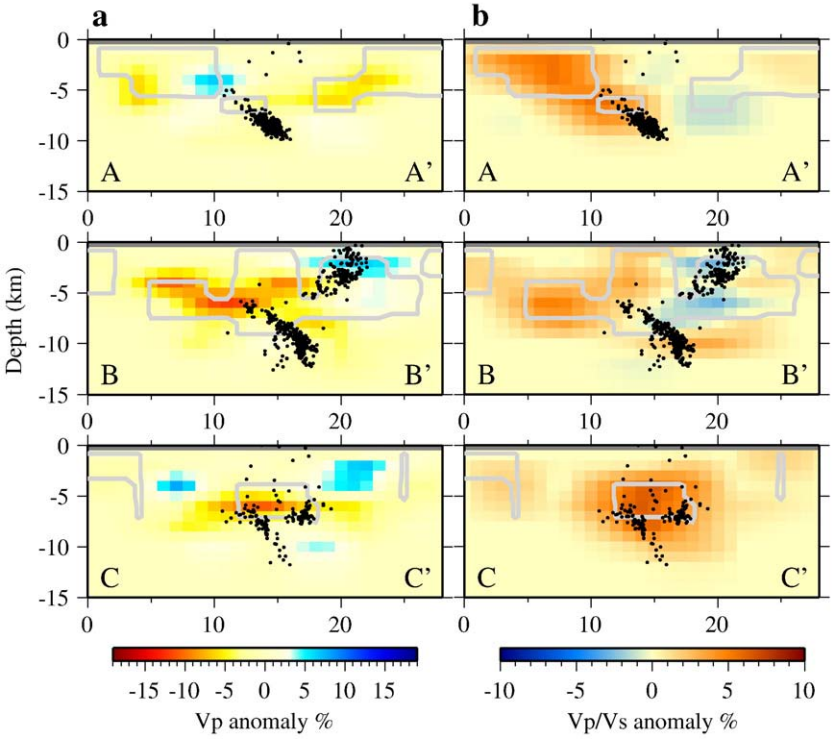

Fig. 9. Cross-sectional views of the velocity anomalies across the fault system. The three panels display profiles that step progressively southward from top to bottom. Transect AA′ shows a profile running across Les Saintes Islands. Transect BB' presents the structure crossing through the middle of the seismic sequence while transect CC′ presents the structure across Roseau Volcano. Blue colors represent fast P-wave velocities or low Vp/Vs ratios, while red colors represent slow P-wave velocities or high Vp/Vs ratios. The grey lines are the isolines of the well-resolved regions (DWS >5000, see Fig. 10). LET hypocenter locations within 5 km of each plane are plotted in black. a) Vp anomaly and b) Vp/Vs anomaly.

Please cite this article as: Bazin, S., et al., The 2004–2005 Les Saintes (French West Indies) seismic aftershock sequence observed with ocean bottom seismometers, Tectonophysics (2010), doi:10.1016/j.tecto.2010.04.005

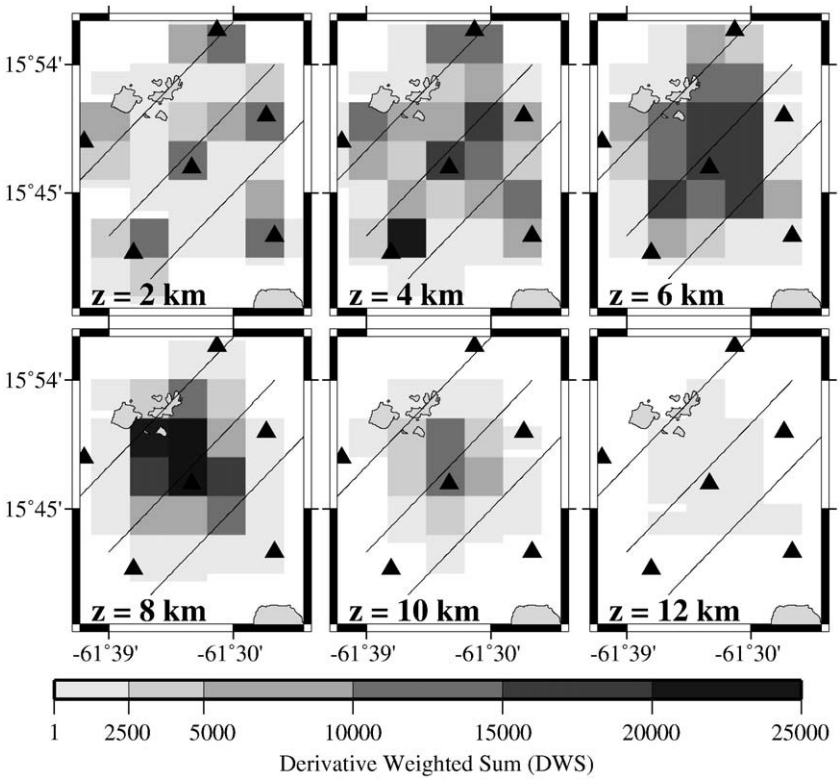

Fig. 10. Map view of derivative weight sum (DWS) values for 6 constant-depth planes. DWS is used as proxy for imaging model resolution. Here, values above 5000 are considered to have adequate resolution (Toomey and Foulger, 1989; Toomey et al., 1994; Haslinger et al., 1999). Black lines mark the locations of the three vertical profiles shown in Fig. 9. Triangles show the positions of the six OBS. Les Saintes and Dominica coastlines are plotted.

6. Aftershock sequence

The 1183 3D-located aftershocks are plotted with the faults and volcanoes in Fig. 11. The average change of epicenter location is 2 km. The locations are now precise enough to image the clustering of aftershocks along planes, allowing us to make a tectonic interpretation. There are two well-defined clusters, with opposite dip. The events of the main cluster align perfectly at depth, on a plane dipping at $50 \pm 3°$ toward the NE. Seismicity on this fault plane is limited to between 5 and 12.6 km depth, with the highest density between 8 and 10 km. The best-fit plane to this cluster has an azimuth of N327°. This plane intersects the surface at the Roseau fault scarp.

The hypocenters computed by OVSG, Harvard, and Geoscope for the main November 21 event lie 15 km apart (Fig. 2) and do not lie on the fault plane identified by the aftershock cluster. The normal mechanisms computed by Harvard and Geoscope are composed of two nodal planes from which it has been so far impossible to decide on the actual fault geometry (Vallée et al., 2005; Delouis et al., 2007). Both CMT nodal planes agree with the N135° azimuth of the normal faults in the Les Saintes graben. From the dip of the relocated fault plane, we propose that the mainshock (21 November 2004, $M_w = 6.3$) and the second major event (14 February 2005, $M_w = 5.8$) both ruptured Roseau fault. The OBS array was not in place during these two main events, but we are able to relocate them with master events that are simultaneously located by the OVSG permanent network using a master-slave technique. Master events are chosen within our 3D-located aftershock dataset with at least 5 P- and 5 S-arrivals in the permanent network and short distances (<5 km) to the slave events. For each slave, three master events verify these conditions. As the slave (the event that we wish to relocate) and its master are close to each other, we can consider similar source-station ray paths. For each master event, we calculate the delay times at the permanent seismic stations by fixing the hypocenter at the position inverted by our LET. These time delays are then applied as station corrections for the relocation of the two slaves. The description of this procedure can be found in Bengoubou-Valérius (2008). The three possible solutions for each of the main events are listed in Table 3 and displayed in Fig. 11a. The deepest solutions do not lie on the fault plane outlined by the relocated aftershocks. Although they do not provide the smallest RMS, our preferred solutions are the shallowest ones (i.e. 8.0 and 8.1 km depth, respectively, for the 21 November and 14 February events) because their projections fall perfectly on the fault plane outlined by the 3D-located cluster. Between these two main shocks, which sit 8 km apart, there seems to be a seismic gap in the aftershock distribution (centered near 15°47′N 61°33′E in Fig. 11a). This lack of seismic activity was already visible between the north and south clusters in the dataset located by the permanent network (Fig. 2) and it persists with the OBS low detection threshold.

The Roseau seismicity distribution is perfectly planar to the north (section 1, Fig. 11b) but widens towards the south (section 3, Fig. 11b). The cloudy cluster may suggest that the postseismic deformation affected several parallel faults, including Le Havre fault, and probably connected at depth with the Roseau main fault. The NE cluster (Fig. 11) probably corresponds to slip on several parallel and smaller fault planes antithetic to Roseau fault (Rodrigues and Souffleur faults). This shallow cluster extends on the Les Saintes plateau suggesting that these antithetic faults continue northward. However, the lack of multibeam bathymetric data in this area cannot confirm this hypothesis. The dipping angle of the antithetic faults cannot be measured with accuracy but it is on the order of 50° as well. Roseau fault and the smaller antithetic ones may connect at depth where a positive Vp anomaly is detected (Fig. 8a, plate $z = 10$km), but the present data cannot confirm it.

The absence of shallow seismicity between the Roseau fault seafloor scarp and the depth of 5 km is not an artifact of the experiment geometry and truly illustrates the fault processes (Fig. 11). However the absence of relocated seismicity below Les Saintes islands, and, south of Roseau volcano is an artifact of the LET

Please cite this article as: Bazin, S., et al., The 2004–2005 Les Saintes (French West Indies) seismic aftershock sequence observed with ocean bottom seismometers, Tectonophysics (2010), doi:10.1016/j.tecto.2010.04.005

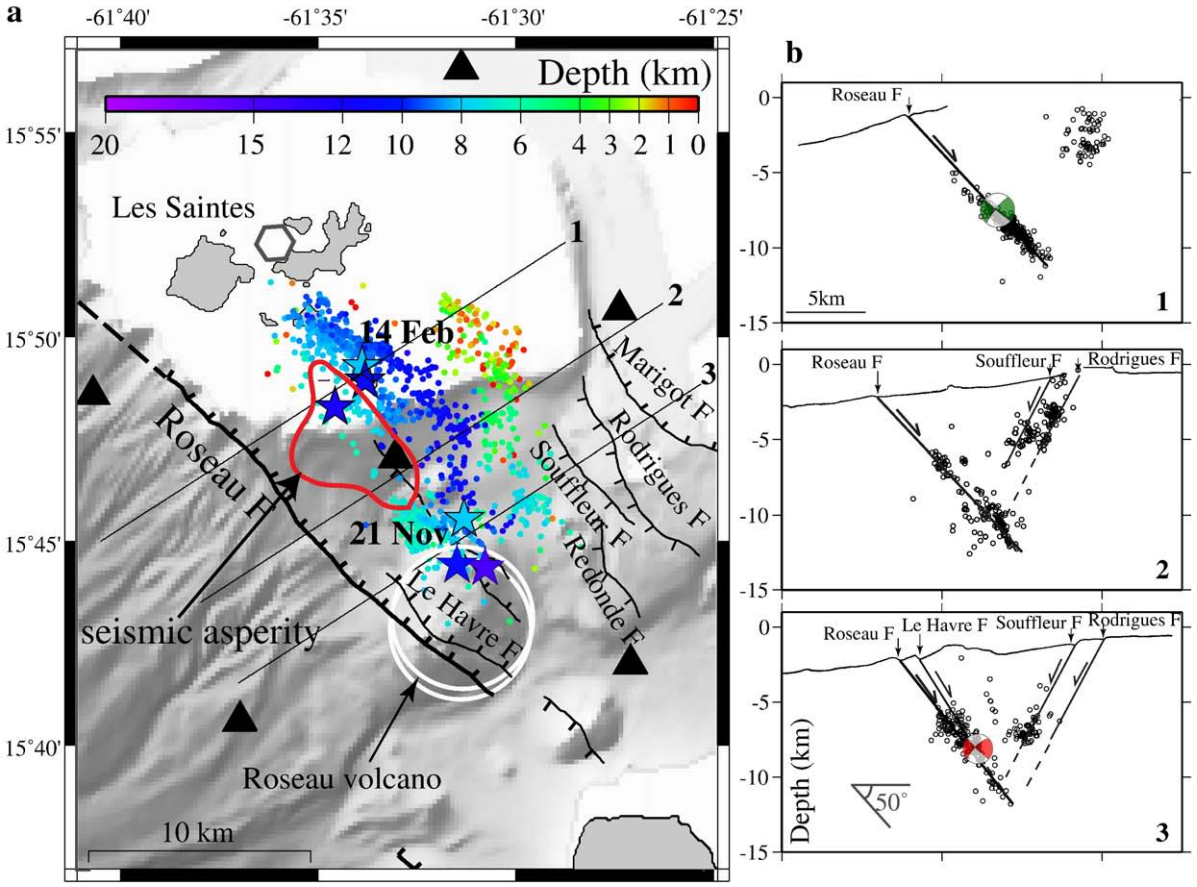

Fig. 11. 3D-located seismicity from the OBS dataset. a) Map view. Simplified fault scarps are from Feuillet (2000). Epicenters are coloured according to the hypocenter depth. Stars indicate the three possible solutions for the mainshock (21 Nov.) and its strongest aftershock (14 Feb.), calculated using slave–master technique (table 3). Our preferred solutions are the shallowest ones, i.e. the lightest blue stars. The patch of high coseismic slip (≥0.5 m) inferred from a teleseismic inversion for the main event (Salichon et al., 2009) is contoured in red. The 3D-located, aftershocks cluster in the lower part of the Roseau fault plane that had not ruptured during the main event. Les Saintes coastlines are plotted and the pentagone indicates the region where a geyser was observed by locals on February 14th (cf Appendix A). The triangles show the positions of the six OBS. b) The three panels display sections that step progressively southward from top to bottom and are perpendicular to the 327°N Roseau cluster azimuth. LET hypocenter locations within 2 km of each plane are plotted in black. The best fitting planes for the Roseau fault cluster and antithetic cluster are drawn; they connect to the surface fault scarps. The antithetic faults do not continue on the Les Saintes plateau but regions above 200 m below sea level were not mapped. Roseau fault dips at 47° for the two northern sections (1 and 2) and at 53° for the southern one (3). A 50° benchmark is shown for reference. The red and green beach balls mark Harvard CMT of the main shock and the main aftershock respectively, at their 3D-relocated positions. They perfectly lie on the LET relocated fault plane.

because events with 180° minimum azimuth coverage are selected for the 3D inversion. There is no seismicity below 12.6 km in the surveyed area, which probably represents the base of the graben formed by the antithetic faults. An antithetic fault was similarly reactivated after the M_s6.6 Kozani-Grevena normal-fault earthquake in 1995, and it connected to the main fault at 12 km depth (Meyer et al., 1996; Chiarabba and Sevaggi, 1997; Hatzfeld et al., 1997). This depth may correspond to the brittle–plastic transition. The typical seismogenic thickness is 15 km but can range from 0 to 40 km in the oceanic crust (Watts and Burov, 2003). Here, the thin seismogenic layer may be controlled by the local geothermal regime as the Les Saintes graben lies along the Lesser Antilles volcanic chain. The thickness of the seismogenic layer influences both the maximum width of grabens and the continuity of the faults (i.e. the maximum segment length) that bound them in extensional provinces (Hayward and Ebinger, 1996). It therefore has important implications for seismic hazard estimation in the region.

Table 3

Latitude	Longitude	Depth (km)	RMS (s)
Three master–slave solutions for the first shock of November 21 2004			
15° 44.43	−61° 31.49	10.85	0.08
15° 45.55	**−61° 31.31**	**8.02**	**0.14**
15° 44.37	−61° 30.78	14.78	0.10
Three master–slave solutions for the strongest aftershock of February 14 2005			
15° 49.29	**−61° 33.88**	**8.11**	**0.12**
15° 48.28	−61° 34.57	12.19	0.11
15° 48.93	−61° 33.81	11.25	0.09

The preferred solutions are in bold. A description of the master–slave procedure can be found in Bengoubou-Valérius (2008).

The main and antithetic clusters were active simultaneously during the 41 days of the OBS deployment; there is no clear temporal evolution within the aftershock sequence. The sequence has a *b*-value of 0.94 (Fig. 4a). Bengoubou-Valérius et al. (2008) computed a regional *b*-value of 1.13 for intraslab events and 1.38 for shallow events. *B*-values ≤1 are typical of magmatic regions but can also be interpreted as regions awaiting a major earthquake. The *b*-value of our dataset is 32% lower than the regional average. It might be due to the fact that the OBS survey took place before the main aftershock on February 14th 2005, or that this active fault system cuts several underwater volcanoes. The ages of these volcanoes are currently unknown, but nearby volcanoes in the Les Saintes archipelago and in the north of Dominica Island were dated to Pliocene Quaternary volcanism (Jacques et al., 1984; Bellon, 1988; Jacques and Maury, 1988).

Please cite this article as: Bazin, S., et al., The 2004–2005 Les Saintes (French West Indies) seismic aftershock sequence observed with ocean bottom seismometers, Tectonophysics (2010), doi:10.1016/j.tecto.2010.04.005

7. Discussions

7.1. Aftershocks, low P-wave velocities and rupture geometry

After 25 days from the mainshock, most of aftershocks along Roseau fault are confined between 8 and 12.6 km and there were none shallower than 5 km. Our master–slave results indicate that the two main ruptures of the seismic sequence most probably started at 8 km depth. The negative Vp anomaly outlines the fault plane from 4 to 8 km depth (Fig. 9a, section BB′) and therefore is mostly located above the mainshock and aftershocks. P- and S-wave velocities in the crust depend on rock mineralogy, temperature, pressure, intrinsic porosity and fracturing as well as the presence of fluids (Christensen, 1996). Low P-wave velocities are typical in faulted regions and we propose that the wide negative Vp anomaly imaged by our LET at 4 to 8 km depth at the graben center (Fig. 8a) outlines sections of Roseau fault where most slip occurred. If we assume that the 21 November rupture reached the surface with a dip angle of 50° and a maximum depth of 8 km, the rupture zone width is on the order of 10.4 km. It is not as wide as previously assumed for the down-dip dimension of the 21 November failure plane (Le Friant et al., 2008; Feuillet et al., in revision) but still compatible with typical rupture dimensions for normal events of such magnitude (Wells and Coppersmith, 1994). Whether the rupture broke the surface or not is difficult to conclude using this dataset only and high-resolution underwater imagery will be necessary to solve this issue. However, as shear stress along a fault plane is required to vanish at the free surface, a shallow earthquake such as the 21 November one is likely to result in surface rupture. Indeed, Le Friant et al. (2008) assumed that the rupture reached the seafloor and successfully reproduced the observed 2–3 m tsunami. They modeled the tsunami wave generated by the November 21 event using a dip angle of 50°, a fault length of 15 km, an epicenter depth of 14 km, a strike angle of 320° and a 1 m uniform slip.

When earthquakes occur, they release the shear stress on the ruptured area and increase the stress beyond their rupture edges, by amount that declines with distance (Mendoza and Hartzell, 1988). Indeed, Chiarabba et al. (2009a) have located aftershocks that cluster around patches of large slip defined by SAR models for the Aquilla earthquake (central Italy). Here, we believe the deep aftershock cluster between 8 and 12.6 km depth was triggered by a stress increase at the rupture bottom–edge following the main shock rupture. The geometry of this deep cluster is in agreement with static Coulomb stress change models (Nostro et al., 1997; Feuillet et al., in revision). As the deep cluster geometry appears planar (Fig. 11b, section 1), we propose that these aftershocks ruptured sections of Roseau fault that had not slipped during the 21 November shock. Salichon et al. (2009) have recently achieved a teleseismic inversion of the 21 November rupture. Without knowing which one of the two nodal planes ruptured they proposed two models. Our preferred solution, model 2 (strike N327° and dip 55°), consists of a main asperity where the maximum slip reaches about 1 m, and a smaller one of 25 cm slip. The main asperity is located NW of the relocated 21 November event, between 8 and 16 km down–dip (which correspond to 6.5–13 km depth assuming the 55° dip, see its projection in Fig. 11a). The smaller asperity is located at the same depth and 10 km to the SE of the main asperity. Although the resolution of the teleseismic inversion is limited and the finite fault model geometry assumed for the rupture (30 km long and 21 km wide plane intersecting the preliminary hypocentral location at 14 km depth) does not coincide with our fault plane solution, the patch of high slip is in agreement with the aftershock pattern. According to Salichon et al. (2009), the 21 November nucleation started at depth (the authors assumed 14 km but we suggest 8 km depth) and propagated up–dip in two patches and probably reached the seafloor. As this event did not rupture the entire width of Roseau fault, aftershocks cluster in the lower part of the fault plane that had not slipped. The aftershock geometry, with the long-lasting cluster near the Les Saintes and a fading cluster near Roseau volcano, is in agreement with the teleseismically inverted rupture showing a main asperity NW of the hypocenter and a smaller one SE of it. Dense monitoring networks have previously imaged diffuse clouds of aftershock which indicate that aftershocks do not always cluster along the main fault planes or aftershock geometries do not always agree with rupture dimensions estimated by geodetic or teleseismic inversions (e.g. Hauksson et al., 1995; Massonnet et al., 1996; Donnellan and Webb, 1998). The present sequence shows a simple planar geometry that matches the surface fault scarp as well as the expected dip and strike determined teleseismically, and which dimensions are consistent with the event magnitude. The reason may be the moderate magnitude of the event and a simple source mechanism as previously suggested by Mellors et al. (1997).

7.2. Fluids

The monochromatic noise recorded by geophones 15 (with lower rate by geophones 13 and 18) may be produced by fluid seepage into the ocean. The proximity of these geophones to the two active faults (OBS 15 is $\leq$3 km away Roseau fault and OBS 13 is $\leq$3.5 km away from Rodrigues fault) favors this interpretation. The island shelf was not mapped during the AGUADOMAR high-resolution bathymetric survey and further mapping would be necessary to identify whether an active fault lies near OBS 18. Moreover, some metallic parts of the OBS mounting were extremely corroded when we recovered the instruments from the seafloor (Fig. 3e). This type of corrosion has not been observed before for such a short deployment time. We infer that the water chemistry near the seafloor was not of normal composition. This is another evidence that the 21 November event ruptured the seafloor. Further sea-bottom investigation would be necessary to solve this enigma. In addition, locals witnessed a bubbling white discharge associated with vapor in the ocean between Terre de Haut and Terre de Bas Islands in the Les Saintes group (location marked on map in Fig. 11a), forming a circular trace that lasted for several hours after the main aftershock (witnesses statements and pictures are presented in Appendix A). Scuba divers also reported zones of higher temperature around the Les Saintes coast, but we were not able to verify this information. Fluids may have been discharged from an underwater fault between these islands. A comparable manifestation was observed at sea on March 17, 1843, 37 days after an M_w8 earthquake NE of Guadeloupe (de Blainville, 1843). A geyser spouting with vapor occurred above Colombie Bank, located along the Morne Piton normal fault, NW of Marie-Galante Island (location marked on map in Fig. 1). Although, the 1843 geyser did not occur shortly after any earthquake, we infer that the Morne Piton fault released a high volume of fluids in a fashion similar to what happened near the Les Saintes Islands on February 14 2005.

Low P-wave velocities are typical in faulted regions while high Vp/Vs anomalies are characteristic of fluid-filled pores and cracks (Eberhart-Phillips and Michael, 1993) or molten bodies (Bazin et al., 2003). Here, the concomitant low Vp and high Vp/Vs anomalies (Fig. 8) could indicate transient fluid in the Roseau fault. In fluid-saturated rocks, high Vp/Vs anomalies may indicate high pore pressure, perhaps because large shallow earthquakes induce changes in the fluid pore pressure that are comparable to stress drop on faults (Nur and Booker, 1972). The pore pressure changes induced by the 21 November event may have caused postseismic fluid flow that slowly decreased the strength of rock (Chiarabba et al., 2009b,c) and resulted in the delayed fracture of the 14 February main aftershock. In addition, large-amplitude long-period motions are observed on broadband data collected during the same aftershock sequence (Jousset and Douglas, 2007). The authors suggest that 5 to 10 s peaks in displacement response spectra are specific oscillating source mechanisms possibly involving fluids within the source. The long-period peak is present during the M_w5.3 aftershock that occurred on November 21 at

Please cite this article as: Bazin, S., et al., The 2004–2005 Les Saintes (French West Indies) seismic aftershock sequence observed with ocean bottom seismometers, Tectonophysics (2010), doi:10.1016/j.tecto.2010.04.005

13:37 TU, 2 h after the main rupture. We suppose that fluids were near the source region prior to the main rupture. Brodsky and Kanamori (2001) have shown that the mechanical effect of viscous fluid lubricating a fault zone has implication on the rupture dynamics. Elevated fluid pressure in a thin film between rock surfaces supports parts of the load reducing the effective normal stress across the fault and, therefore, can facilitate earthquake nucleation. Byerlee (1993) has proposed a compartment model to explain the cyclic behaviour of earthquake triggering: during an earthquake, the fault zone compacts and water flows into the damaged and porous country rock until the fault zone pore pressure reaches the country rock hydrostatic pressure. This new state can trigger another earthquake. Overall, fluid moving in and out of the fault zone could be the driving mechanism for such a long-lasting aftershock sequence. The negative Vp/Vs anomaly in the region of the antithetic Rodrigues and Souffleur faults suggests that fluids may not be involved in their rupture process. For that reason, the activity on the antithetic faults has ended after a few months. In comparison, the seismic sequence that followed the M_s6.2 strike–slip Redonda event that occurred north of Montserrat Island on March 16 1985, lasted only for a few months (Girardin et al., 1991). A late M_s5.2 aftershock occurred on February 12 1986 and was followed by a short aftershock sequence. We propose that the difference between the >5 year-long Les Saintes sequence and the 1 year-long Redonda sequence is caused by different fluid regimes. The reason why Roseau fault is lubricated while Redonda fault seems not, could be due to its occurrence in a volcanic region. It would be interesting in the future to identify the source of these high-pressure fluids by isotropic studies and define whether they come from the country rock at the base of the fault.

8. Conclusions

The 21 November 2004 M_w6.3 Les Saintes earthquake induced a very long-lasting aftershock sequence. We have successfully applied three-dimensional seismic tomographic inversions to an OBS dataset collected during 41 days of the aftershock sequence. Our results indicate that Roseau fault triggered the 21 November earthquake and that the seismicity is not concentrated along one single fault but also along several antithetic normal faults in the Les Saintes graben. The seismogenic thickness is lower than normal, probably due to the geothermal regime in this volcanic region. The relocated aftershock sequence and the velocity anomalies correspond to the continuation of Roseau fault at depth. The fault plane azimuth of the aftershock distribution is N327° and the dip is 50° toward the NE, which corresponds well with the surface alignment of Roseau Fault. The deep aftershock cluster is in agreement with the slip distribution of the 21 November rupture. The inverted Vp/Vs is 1.81, much higher than the regional value of 1.73. A positive Vp/Vs anomaly in the region of the Roseau fault plane might indicate pore-fluid flow. We suggest that mainshock-induced pore pressure changes controlled the timing of the strongest aftershock (75 days later), 8 km further north on the same fault. A negative Vp/Vs anomaly in the region of the antithetic Rodrigues and Souffleur faults might indicate a different state of pore pressure distribution than for Roseau fault. This study illustrates the scientific benefits of post-earthquake surveys. Although it was a challenge to mount this marine experiment, it provides a dataset that is crucial to understanding the region's seismotectonics. Further marine surveys are needed to address, among other questions, the possibility that the November 21, 2004 rupture reached the seafloor, and the presence of fluid seepage along the fault scarps.

Acknowledgments

We thank Captain N. Radenne and the crew of the *Kahouanne* for the success of the two legs of the GUADOBS marine experiment. We thank L. Beguery and O. Aouji for rapidly preparing and deploying the OBSs. We are grateful to the Guadeloupe authorities and Phares et Balises for providing the vessel and also to SIO team for providing OBS batteries that permitted this rapid response experiment. We thank OVSG technical team for the seismic analysis of the regional network. We thank the IPGP seismic crisis team that helped with the organization and INSU for financing airfare and equipment. We thank R. Poujardieu for relocating the OBS coordinates during a summer internship and C. Deplus for providing the AGUADOMAR bathymetric grid. We acknowledge the use of TOMO2GMT shareware of S. Husen and F. Haslinger. Figs. 1, 2, 5, 8, 9, 10, and 11 were created with GMT (Wessel and Smith, 1995). Useful suggestions to improve the paper were given by the editor and two anonymous reviewers. IPGP contribution 2614.

Appendix A. Supplementary data

Supplementary data associated with this article can be found, in the online version, at doi:10.1016/j.tecto.2010.04.005.

References

Allen, R.V., 1978. Automatic earthquake recognition and timing from single traces. Bull. Seismol. Soc. Am. 68, 1521–1532.
Bazin, S., Harding, A.J., Kent, G.M., Orcutt, J.A., Singh, S.C., Tong, C.H., Pye, J.W., Barton, P.J., Sinha, M.C., White, R.S., Hobbs, R.W., van Avendonk, H.J.A., 2003. A three-dimensional study of axial low velocity region beneath the 9°03′N overlapping spreading center. Geophys. Res. Lett. 30, 1039–1042.
Beauducel, F., Anténor-Habazac, C., Bazin, S., de Chabalier, J.-B., Nercessian, A., Feuillet, N., Jacques, E., Bertil, D., Boudon, G., Le Friant, A., Tapponnier, P., Hirn, A., Lépine, J.-C., Bernard, P., Komorowski, J.-C., King, G.C.P., 2005. The Mw 6.3 earthquake of Les Saintes (Guadeloupe) on November 21, 2004. IAVCEI European Seismological Commission Annual Workshop, Saint-Claude Guadeloupe, Sep. 2005.
Bellon, H., 1988. Reconnaissance Chronologique des deux premières phases d'activité volcanique en Dominique (Petites Antilles). C. R. Acad. Sci. 306, 1487–1492.
Bengoubou-Valérius, M., 2008. Contribution à la connaissance de l'Aléa sismique dans les Antilles Françaises. Univ. des Antilles et de la Guyane, Ph.D. thesis, 189 pp.
Bengoubou-Valérius, M., Bazin, S., Bertil, D., Beauducel, F., Bosson, A., 2008. CDSA: a new seismological data center for French Lesser Antilles. Seismol. Res. Lett. 79, 90–102.
Bernard, P., Lambert, J., 1988. Subduction and seismic hazard in the Northern Lesser Antilles—revision of the historical seismicity. Bull. Seismol. Soc. Am. 78, 1965–1983.
Bertil, D., Bazin, S., Mallarino, D., Beauducel, F., 2004. Séisme des Saintes — Rapport de Synthèse. Centre de Données Sismologiques des Antilles, 8 décembre 2004. 36 pp.
Bouysse, Ph., 1980. Sur l'existence d'un volcan sous-marin dans l'archipel de la Guadeloupe. BRGM, Rapport 80 SGN 084 MAR. 36 pp.
Vallée, M., Delouis, B., Bazin, S., 2005. Rupture process of the mainshocks of the Guadeloupe, West Indies, seismic crisis (November 2004–February 2005). Workshop on fracture dynamics: Theory and application to earthquakes, Madrid. .
Brodsky, E., Kanamori, H., 2001. Elastohydrodynamic lubrication of faults. J. Geophys. Res. 106, 16 357–16 374.
Byerlee, J., 1993. Model for episodic flow of high-pressure water in fault zones before earthquake. Geology 21, 303–306.
Cara, M., Bertil, D., Feuillet, N., Jacques, E., Tapponnier, P., Guéguen, P., Bengoubou-Valérius, M., Sira, C., Lebrun, B., Beauducel, F., 2005. Séisme des Saintes (Guadeloupe) du 21 novembre 2004, note préliminaire. BCSF2005-NP3. 62 pp.
Cara, M., Alasset, P.-J., Sira, C., 2008. Magnitude of historical earthquakes, from macroseismic data to seismic waveform modelling: application to the Pyrenees and a 1905 earthquake in the Alps. Hist. Seismol. 2, 369–384. doi:10.1007/978-1-4020-8222-1.
Chiarabba, C., Sevaggi, G., 1997. Structural control on fault geometry: example of the Grevena Ms 6.6, normal faulting earthquake. J. Geophys. Res. 102, 22 445–22 457.
Thurber, C.H., 1983. Earthquake locations and three-dimensional crustal structure in the Coyote lake area, Central, California. J. Geophys. Res. 88, 8226–8236.
Chiarabba, C., Amato, A., Anselmi, M., Baccheschi, P., Bianchi, I., Cattaneo, M., Cecere, G., Chiaraluce, L., Ciaccio, L., De Gori, M.G., De Luca, P., Di Bona, G., Di Stefano, M., Faenza, R., Govoni, A., Improta, L., Lucente, F.P., Marchetti, A., Margheriti, L., Mele, F., Michelini, A., Monachesi, G., Moretti, M., Pastori, M., Piana Agostinetti, N., Piccinini, D., Roselli, P., Seccia, D., Valoroso, L., 2009a. The 2009 L'Aquila (central Italy) Mw 6.3 earthquake: Main shock and aftershocks. Geophys. Res. Lett. 36. doi:10.1029/2009GL039627.
Chiarabba, C., De Gori, P., Boschi, E., 2009b. Pore-pressure migration along a normal-fault system resolved by time-repeated seismic tomography. Geology 37 (1), 67–70. doi:10.1130/G25220A.1.
Chiarabba, C., Piccinini, D., De Gori, P., 2009c. Velocity and attenuation tomography of the Umbria Marche 1997 fault system: evidence of a fluid-governed seismic sequence. Tectonophysics. doi:10.1016/j.tecto.2009.04.004.
Christensen, N.I., 1996. Poisson's ratio and crustal seismology. J. Geophys. Res. 101, 3139–3156.
Clément, C., Bernard, P., Viodé, J.-P., Antenor-Habazac, C., Lépine, J.-C., Beauducel, F., 2001. Compilation et validation du catalogue de sismicité des observatoires IPGP des Antilles Françaises. Rapport MATE-IPGP. 95 pp.

Please cite this article as: Bazin, S., et al., The 2004–2005 Les Saintes (French West Indies) seismic aftershock sequence observed with ocean bottom seismometers, Tectonophysics (2010), doi:10.1016/j.tecto.2010.04.005

Constable, S.C., Orange, A.S., Hoversten, G.M., Morrison, H.F., 1998. Marine magnetotellurics for petroleum exploration, part 1, a seafloor equipment system. Geophysics 63, 816–825.
de Blainville, C., 1843. Sur un volcan qui a fait éruption entre la Guadeloupe et Marie-Galante. C. R. Acad. Sci. 16 (19), 1083–1084.
Delouis, B., Vallée, M., Cruz-Atienza, V., 2007. The Mw = 6.3 Saintes earthquake (West Indies): source kinematics determination and uncertainties in a poorly known crustal structure. Geophys. Res. Abstr. 9, 10050.
DeMets, C., Jansma, P.E., Mattioli, G.S., Dixon, T.H., Farina, F., Bilham, R., Calais, E., Mann, P., 2000. GPS geodetic constraints on Caribbean–North America plate motion. Geophys. Res. Lett. 27, 437–440.
Deplus, C., Le Friant, A., Boudon, G., Komorowski, J.-C., Villemant, B., Harford, C., Ségoufin, J., Cheminée, J.-L., 2001. Submarine evidence for large-scale debris avalanches in the Lesser Antilles Arc. Earth Planet. Sci. Lett. 192, 145–157.
Donnellan, A., Webb, F.H., 1998. Geodetic observations of the M 5.1 January 29, 1994 Northridge aftershock. Geophys. Res. Lett. 25, 667. doi:10.1029/98GL50323.
Dorel, J., 1978. Sismicité et structure de l'arc des Petites Antilles et du bassin Atlantique. Ph.D. thesis, Université Pierre et Marie Curie, 326 pp.
Dorel, J., Eschenbrenner, S., Feuillard, M., 1974. Profils sismiques dans les Petites Antilles. Ann. Geophys. 30, 117–126.
Eberhart-Phillips, D., 1990. Three-dimensional P and S velocity structure in the Coalinga region, California. J. Geophys. Res. 95, 15 343–15 363.
Eberhart-Phillips, D., Michael, A.J., 1993. Three-dimensional velocity structure and seismicity in the Parkfield region, central California. J. Geophys. Res. 98, 15 737–15 758.
Eberhart-Phillips, D., Reyners, M., 1997. Continental subduction and three-dimensional crustal structure: the northern South Island, New Zealand. J. Geophys. Res. 102, 11 843–11 861.
Evans, J.R., Eberhart-Phillips, D., Thurber, C.H., 1994. User's manual for SIMULPS12 for imaging Vp and Vp/Vs: a derivate of the Thurber tomographic inversion SIMUL3 for local earthquakes and explosions. U.S. Geol. Surv. Open File Rep., 94-431, 101pp.
Feuillet N., 2000. Sismotectonique des Petites Antilles, Liaison entre activité sismique et volcanique, Ph.D. thesis, Université Paris 7, 283 pp.
Feuillet, N., Manighetti, I., Tapponnier, P., 2001. Extension active perpendiculaire à la subduction dans l'arc des Petites Antilles (Guadeloupe). C. R. Acad. Sci. 333, 583–590.
Feuillet, N., Tapponnier, P., Manighetti, I., Villemant, B., King, G., 2004. Differential uplift and tilt of Pleistocene reef platforms and Quaternary slip rate on the Morne–Piton normal fault (Guadeloupe, French West Indies). J. Geophys. Res. 109. doi:10.1029/2003JB002496.
Feuillet, N., Beauducel, F., Jacques, E., Bazin, S., Tapponnier, P., King, G.C.P., The Mw = 6.3, November 21, 2004, Les Saintes earthquake (Guadeloupe): tectonic setting and static stress modeling. In revision.
Girardin, N., Feuillard, M., Viodé, J.-P., 1991. Réseau régional sismique de l'arc des Petites Antilles: sismicité superficielle (1981–1988). Bull. Soc. Géol. Fr. 162 (6), 1003–1015.
Haslinger, F., Kissling, E., Ansorge, J., Hatzfeld, D., Papadimitriou, E., Karakostas, V., Makropoulos, K., Kahle, H.-G., Peter, Y., 1999. 3D crustal structure from local earthquake tomography around the Gulf of Arta (Ionian region, NW Greece). Tectonophysics 304, 201–218.
Hatzfeld, D., Karakostas, V., Ziazia, M., Selvaggi, G., Leborgne, S., Berge, C., Guiguet, R., Paul, A., Voidomatis, P., Diagnourtas, D., Kassaras, I., Koutsikos, I., Makropoulos, K., Azzara, R., Di Bona, M., Baccheschi, S., Bernard, P., Papaioannou, C., 1997. The Kozani–Grevena (Greece) earthquake of 13 May 1995 revisited from a detailed seismological study. Bull. Seismol. Soc. Am. 87, 463–473.
Hauksson, E., Jones, L.M., Huttor, K., 1995. The 1994 Northridge earthquake sequence in California: seismological and tectonic aspects. J. Geophys. Res. 100, 12 3335–12 355.
Havskov, J., Ottemöller, L., 2005. SEISAN: the earthquake analysis software. Version 8.1, User's manual, University of Bergen, Norway, 259 pp.
Hayward, N.J., Ebinger, C.J., 1996. Variations in the along-axis segmentation of the Afar Rift system. Tectonics 15, 244–257.
IPGP, 2009. Bilan mensuel de l'activité volcanique de la Soufrière de Guadeloupe et de la sismicité régionale. Monthly Public Reports of OVSG-IPGP, Institut de Physique du Globe de Paris, Gourbeyre, 2004–2009.
Jacques, D., Maury, R.C., 1988. Carte géologique du département de la Guadeloupe: Les Saintes 1/20 000. BRGM, Orléans. 28 pp.
Jacques, D., Maury, R.C., Bellon, H., 1984. Géologie et géochronologie 40K–40Ar des îles des Saintes (Guadeloupe). C. R. Acad. Sci. 299, 721–726.
Japan Meteorological Agency, 2004. The seismological and volcanological bulletin of Japan for January 2004. http://www.fnet.bosai.go.jp/event2004.
Jousset, P., Douglas, J., 2007. Long-period earthquake ground displacements recorded on Guadeloupe (French Antilles). Earthquake Eng. Struct. Dyn. 36, 949–963.
Kissling, E., Ellsworth, W.L., Eberhart-Phillips, D., Kradolfer, U., 1994. Initial reference models in earthquake tomography. J. Geophys. Res. 99, 19635–19646.
Kissling, E., Kradolfer, U., Maurer, H., 1995. VELEST user's guide-short introduction. Institute of Geophysics and Swiss Seismological Service, ETH, Zurich. 25 pp.
Kissling, E., Husen, S., Haslinger, F., 2001. Model parameterization in seismic tomography: a choice of consequences for the solution quality. Phys. Earth Planet. Inter. 123, 89–101.
Le Friant, A., Heinrich, P., Boudon, G., 2008. Field survey and numerical simulation of the 21 November 2004 tsunami at Les Saintes (Lesser Antilles). Geophys. Res. Lett. 35, L12308. doi:10.1029/2008GL034051.
Lee, W.H., Lahr, J.H., 1975. HYPO71 (revisited): a computer program for determining hypocenter, magnitude and first motion pattern of local earthquakes. U.S. Geol. Surv., Open File Rep., Menlo Park, California, pp. 75–311.
Lienert, B.R., 1994. HYPOCENTER 3.2: a computer program for locating earthquakes locally, regionally and globally. Tech. rep., Hawaii Institute of Geophysics and Planetology, Honolulu, 74 pp.
Massonnet, D., Feigl, K.L., Vadon, H., Rossi, M., 1996. Coseismic deformation field of the M = 6.7 Northridge California earthquake of January 17, 1994 recorded by two radar satellites using interferometry. Geophys. Res. Lett. 23, 969–972.
Mellors, R.J., Vernon, F.L., Pavlis, G.L., Abers, G.A., Hamburger, M.W., Ghose, S., Iliasov, B., 1997. The Ms = 7.3 1992 Suusamyr, Kyrgyzstan, earthquake: 1. Constraints on fault geometry and source parameters based on aftershocks and body-wave modeling. Bull. Seismol. Soc. Am. 87, 11–22.
Mendoza, C., Hartzell, S.H., 1988. Aftershock patterns and main shock faulting. Bull. Seismol. Soc. Am. 78, 1438–1449.
Meyer, B., Armijo, R., Massonet, D., de Chabalier, J.-B., Delacourt, C., Ruegg, J.-C., Achache, J., Briole, P., Papanastassiou, D., 1996. The 1995 Grevena (Northern Greece) earthquake: fault model constrained with tectonic observations and SAR interferometry. Geophys. Res. Lett. 23, 2677–2680.
Nostro, C., Cocco, M., Belardinelli, M.E., 1997. Static stress changes in extensional regimes: an application to Southern Apennines (Italy). Bull. Seismol. Soc. Am. 87, 234–248.
Nur, A., Booker, J.R., 1972. Aftershocks caused by pore fluid flow? Science 175 (4024), 885–887.
Pontoise, B., Hello, Y., 2002. Monochromatic infra-sound waves recorded offshore Ecuador: possible evidence of methane release. Terra Nova 14, 1–11.
Salichon, J., Lemoine, A., Aochi, H., 2009. Validation of teleseismic inversion of the 2004 Mw 6.3 Les Saintes, Lesser Antilles, earthquake by 3D finite-difference forward modelling. Bull. Seismol. Soc. Am. 99, 3390–3401.
Stein, S., Engeln, J.F., Wiens, D.A., Fujita, K., Speed, R.C., 1982. Subduction seismicity and tectonics in the Lesser Antilles arc. J. Geophys. Res. 87 (B10), 8642–8664.
Toomey, D.R., Foulger, G.R., 1989. Tomographic inversion of local earthquake data from the Hengill-Grensdalur Central volcano complex, Iceland. J. Geophys. Res. 94, 17 497–17 510.
Toomey, D.R., Purdy, S.C., Purdy, G.M., 1994. Tomographic imaging of the shallow crustal structure of the East Pacific rise at 9°30′N. J. Geophys. Res. 99, 24 135–24 157.
Wadati, K., 1933. On the travel time of seismic wave. Geophys. Mag. 7, 87–153.
Watts, A.B., Burov, E.B., 2003. Lithospheric strength and its relationship to the elastic and seismogenic layer thickness. Earth Planet. Sci. Lett. 213, 113–131.
Wells, D.L., Coppersmith, K.J., 1994. New empirical relationships among magnitude, rupture length, rupture width, rupture area, and surface displacement. Bull. Seismol. Soc. Am. 84, 974–1002.
Wessel, P., Smith, W.H.F., 1995. New version of the generic mapping tools released. Eos Trans. AGU. 76, 329.

Please cite this article as: Bazin, S., et al., The 2004–2005 Les Saintes (French West Indies) seismic aftershock sequence observed with ocean bottom seismometers, Tectonophysics (2010), doi:10.1016/j.tecto.2010.04.005